# Numerical Simulation of a Cable-Stayed Bridge Subjected to Ship Collision

Xiao-Qing Zhou[1], Jia-Zhu Hong[1], and Yong Xia[2*]

[1]*College of Civil and Transportation Engineering, Shenzhen University, China*

[2]*Department of Civil and Environmental Engineering, The Hong Kong Polytechnic University, Hong Kong, China*

*Corresponding author, email: ceyxia@polyu.edu.hk

## Abstract

Long-span cable-stayed bridges are subjected to the risk of collision from passing ships. Conducting experimental study on the collision of bridges and vessels is difficult due to high cost and limited space. In the present paper, the behavior of a 1018-m long-span cable-stayed bridge subjected to ship collisions is numerically studied. Finite element models of the entire bridge and ships are established. Four different dead weight tonnages (DWT), namely, 2700, 12000, 30000, and 75000 t, with impact velocities of 1 m/s to 6 m/s are investigated. The complete collision process under different loading scenarios is simulated, from which the collision force, bridge responses and local damage are obtained. The calculated collision force is significantly affected by the impact velocity and DWT, and exhibits a linear relationship with the impact velocity. Comparison with design codes shows that different codes vary significantly in estimating the collision force and Eurocode provides most accurate results. The effect of the material model on the collision force is also studied. This numerical study provides a reference for the ship collision design of long-span cable-stayed bridges.

**Keywords:** ship–bridge collision, long-span cable-stayed bridge, numerical simulation, finite element method, collision force.

## 1. Introduction

To meet the increasing economic demand and improve transportation efficiency, long-span bridges have received increasing application interest[1-3]. Cable-stayed bridges, with merits of relatively low cost and design flexibility, are widely adopted all over the world. These bridges usually span over busy navigation channels and are thus subjected to high collision risk from passing vessels. Reportedly, at least one serious ship collision accident occurs per year worldwide[4]. For example, the Interstate 40 bridge disaster occurred southeast of Webbers Falls, Oklahoma, United States on May 26, 2002 when freight barges on the Arkansas River collided with a pier of the bridge, causing a section of the bridge to collapse, killing 14 people, and injuring another 11. In 2007, a cargo struck one pier of the Jiujiang Bridge, causing two spans to collapse and killing nine people.

The accident of a ship hitting a bridge may result in a ship overturning accident and serious damage or even collapse of the bridge[5–8]. These accidents often cause casualties, bring serious direct and indirect economic losses, and have a huge social impact. For a large-scale bridge on the main line of traffic, a ship collision will suspend the traffic and cause significant losses. For example, a tugboat scratched the bottom of the Kap Shui Mun Bridge in Hong Kong, triggering an alarm and paralyzing the city's international flight hub for hours[9]. Therefore, studying the behavior of bridges subjected to ship collisions is important in ensuring their safety.

A pioneering research work on the ship–bridge collision was conducted in 1959 by Minorsky[10] who performed 26 ship–ship collision tests and derived the relationship between the ship deformation and dissipated energy during collision. Later, Woisin[11] carried out further experimental studies and proposed a new formula of the ship deformation and dissipated energy relationship. Those experimental studies provided valuable and reliable ship–ship collision data and improved the understanding of the collision process. The study of ship–bridge collision had been in relatively slow

progress until the collapse of the Sunshine Skyway Bridge in 1980[12]. This event was a major turning point in awareness and increased the concern for the safety of bridges crossing navigable waterways. Ship collision design principles and specifications have been developed since 1983[13], and Guide Specification and Commentary for Vessel Collision Design of Highway Bridges[14] was published by the American Association of State Highway and Transportation Officials (AASHTO). Eurocode 1[15] specifies the ship collision to bridge design, including the method for calculating the impact load. Other countries have also issued similar regulations[16,17]. These design codes recommend a static collision force to be applied to the bridge. Although the recommended method is convenient for engineers, simplifying the collision process and ignoring the dynamic effects may result in significant errors and underestimate the collision effect.

The ship–bridge collision test can obtain an accurate collision force time-history, the overall deformation of the bridge, and the damage of the ship and bridge, which are important bases of understanding the ship–bridge collision problem. Meier-Dornberg[18] took the European Type IIa barge as a prototype and used 1:4.5 and 1:6 scaled ships for static and dynamic collision tests. The relationship between the impact force and energy and the plastic deformation of the hull during collision were obtained. Vredeveldt and Wevers[19] carried out a full-scale ship–bridge collision test. In the test, two inland oil tankers hit piers at a collision speed of 4.2 m/s. The collision force time history, impact depth, hull strain, and other data were recorded during the collision, providing a valuable reference for the subsequent research on collision performance data. The University of Florida[20] conducted multiple full-scale ship collision tests on the to-be-removed Bryant Pattern bridge. The tests impacted the two piers of the bridge separately, and the collision force, the deformation of the barge, and the dynamic response of the piers and the foundation during the collision were measured. Compared with the American Code[14], the simplified calculation formula of the ship's collision force in the code had errors under both high and low speed conditions. Meanwhile, the ship's impact

on the bridge can be transmitted from the struck bridge pier to the adjacent pier through the superstructure.

Conducting a ship-collision experiment in the laboratory is very expensive, and field testing is almost impossible. Therefore, numerical simulation might be the most convenient, efficient, and economic approach. Nonlinear finite element (FE) codes, such as LS-DYNA[21-29] , ABAQUS[30,31], and ADINA[32] have been widely used for ship collision analyses. Among them, LS-DYNA [33,34] is the most popular software, and most of the numerical simulations focused on the collision force of barge collisions with bridge piers. For example, Yuan and Harik[21,22] used LS-DYNA to study the collision force between bridge piers and ships, considering different pier geometries. Sha and Hao[23] also used LS-DYNA to simulate the impact of barges of different masses on square piers at different speeds. The collision force time-history curve and the collision depth of the barge were analyzed. A simplified formula for quickly predicting the time history curve of the barge collision force was obtained. Later, Sha and Hao[24] numerically simulated multiple scenarios of a barge hitting a circular cross-section pier and analyzed the effects of the barge's mass and speed, the pier's diameter and height, and other factors on the collision force. Most of these studies mainly focused on the collision force caused by ship–bridge collision and ignored the effect of the entire bridge. Therefore, the FE model usually includes bridge piers only without considering the entire bridge model. Recently, entire bridge models were constructed to consider the superstructure interaction [1,35-39]. In particular, refined FE nonlinear analysis have been conducted to study the behavior and damage assessment of ship-bridge collisions [36-40]. At the same time, concrete bridges under multi-hazard were also been studied[41-42] and the bridge protection methods were proposed [43-44].

This study investigates the ship collision behavior of a 1018-m long main span cable-stayed bridge using the LS-DYNA software. The FE models of the entire bridge and ships are established. Different ship tonnages at different impact velocities are considered. The intensive dynamic collision process is simulated. The resulting

collision forces are then compared with those from different design codes. The influence of different concrete material models on the impact force is studied. Global responses and local damage of the bridge are also calculated. The results obtained in this study can assist engineers in improving the design and safety assessment of long-span cable-stayed bridges subjected to ship collision.

## 2. Description of the cable-stayed bridge

The bridge (shown in Fig. 1) is a double-plane cable-stayed bridge that carries dual three-lane highway traffic. The total length of the bridge is 1,596 m, with a span arrangement of 69.25 m + 70 m + 70 m + 79.75 m + 1,018 m + 79.75 m + 70 m + 70 m + 69.25 m. The main structural components include 2 bridge towers, 8 transition piers, 2 main girders, and 122 pairs of cables. The bridge strides on the busy navigation channel to the Hong Kong International Terminals, which was the largest container port in terms of Twenty-foot Equivalent Unit worldwide and now is the 7th largest. Many container carriers pass underneath the bridge, and the ship collision is one concern of the bridge safety.

The 298-m tall bridge towers are of single pole type, and the cross sections are shown in Fig. 2. At ground level, it is shaped like a circular base with a diameter of 18 m and a straight edge of 6 m. The straight line and radius of the curved portion decrease with the height of the tower. At the deck height (74 m), the tower is round and has a diameter of 14 m, and the diameter shrinks to 11 m at 175 m above the ground and remains constant until the tower top. The wall thickness of the tower is constant at 2 m above the deck level, reduces to 1.4 meters at the 175-m level, and remains constant thereafter. The piers are designed with twin hollow box sections, which are 10 m wide and 4 m deep, with 0.5- and 1-m thicknesses, as shown in Fig. 3. A twin deck system is adopted in this bridge, with a steel girder in the main span and a pre-stressed concrete girder in the side spans. Both the main and side spans have a total width of 53.5 m, with two 21-m wide decks connected by 5.75-m steel or concrete girders, as shown in Fig. 4. The

bridge includes 112 pairs of cables twisted with different numbers of wires, as shown in Fig. 1. The cables have an anchorage distance of 18 m in the main span and 10 m in the side span. The shortest cable has an initial length of 112.66 m and longest of 539.02 m. The bridge has been numerically studied under blast loads[45,46].

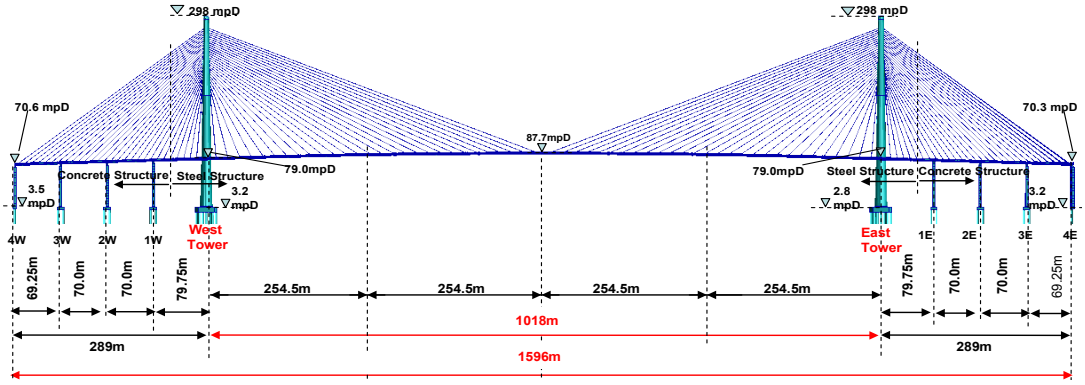


Fig. 1. Configuration of the bridge.

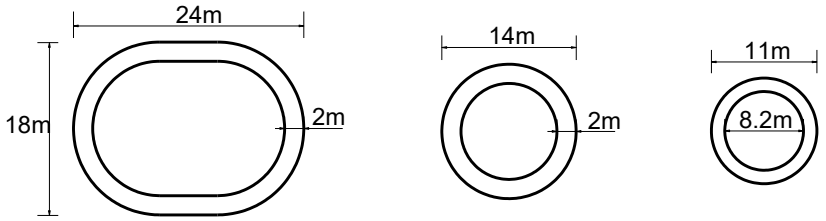


(a) Ground level (b) At 74 m high (c) At 175 m high

Fig. 2. Cross section of the tower.

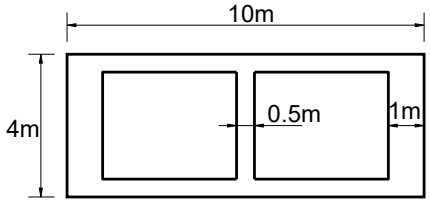


Fig. 3. Cross section of the piers.

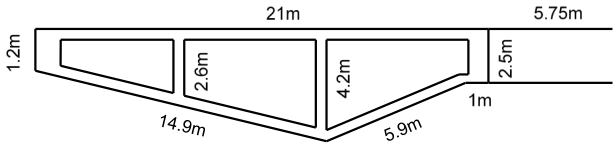


(a) Cross section of the pre-stressed concrete girder

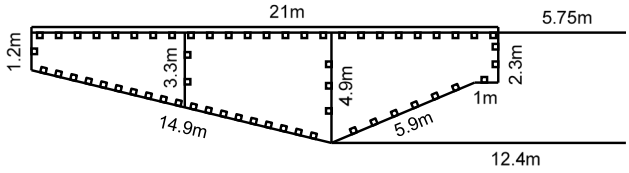


(b) Cross section of the steel girder

Fig. 4. Cross section of the girders.

## 3. Finite element modeling

### *3.1. Bridge model*

#### *3.1.1. Geometry of the bridge model*

The full bridge model constructed is shown in Fig. 5. In this model, the two-node Belytschko–Schwer resultant beam element is used to simulate the bridge deck, beams, towers, side span piers, and piles. The section characteristics of the members are accurately defined by inputting the specific section information. The cables are simulated using tension-only cable elements. The initial tension of the cable is introduced by defining the initial elongation of the cable element. The cable forces are calculated from the elongation and then assigned to the cable elements. The initial tension varies from 3.0 MN for the shortest cables in the main span to 10.2 MN for the longest cables in the side span. Rigid connections are used between the piers and the girder, and the mass of complex connectors is considered by using an additional mass at the midpoint of the beam. The properties of the soil layers are listed in Table 1. The soil-pile interaction is modelled using two-node discrete soil springs, each being 5 m

long. One end of the soil spring is connected to the pile through a common node, and the other end is connected to a fixed node. The soil spring is assumed to be liner and modeled by *MAT_ELASTIC_SPRING_DISCRETE_BEAM with stiffness and viscous damping inputs. The viscous damping coefficient is set to a constant 0.03 for all soil springs. The stiffness of the spring is determined by the displacement method. Various cases of the soil-pile model and the spring stiffness are given in Table 2.

Table 1. Properties of the soil layers.

| Layer | Lower Altitude | Upper Altitude | Density ($kg/m^3$) | Shear Modulus (Pa) | Poisson's Ratio | Angle of Internal Friction (radian) | Cohesion Value (Pa) |
|---|---|---|---|---|---|---|---|
| Layer 1 | -30.00 | 3.20 | 1840 | $3.571\times10^8$ | 0.40 | 0.524 | $1.796\times10^4$ |
| Layer 2 | -45.00 | -30.00 | 2000 | $1.034\times10^{10}$ | 0.45 | 0.628 | $3.592\times10^4$ |
| Layer 3 | -61.00 | -45.00 | 2200 | $2.759\times10^{10}$ | 0.45 | 0.716 | $7.185\times10^4$ |

Table 2. The soil-pile model and the spring stiffness.

| Case | Pile diameter (m) | Soil layer | Stiffness per unit length ($N/m^2$) |
|---|---|---|---|
| 1 | 2.8 | Layer 1 | $4.42\times10^7$ |
| 2 | 2.8 | Layer 2 | $1.95\times10^9$ |
| 3 | 2.8 | Layer 3 | $5.69\times10^9$ |
| 4 | 2.5 | Layer 1 | $4.02\times10^7$ |
| 5 | 2.5 | Layer 2 | $1.80\times10^9$ |
| 6 | 2.5 | Layer 3 | $5.41\times10^9$ |
| 7 | 2 | Layer 1 | $3.31\times10^7$ |
| 8 | 2 | Layer 2 | $1.60\times10^9$ |
| 9 | 2 | Layer 3 | $4.38\times10^9$ |

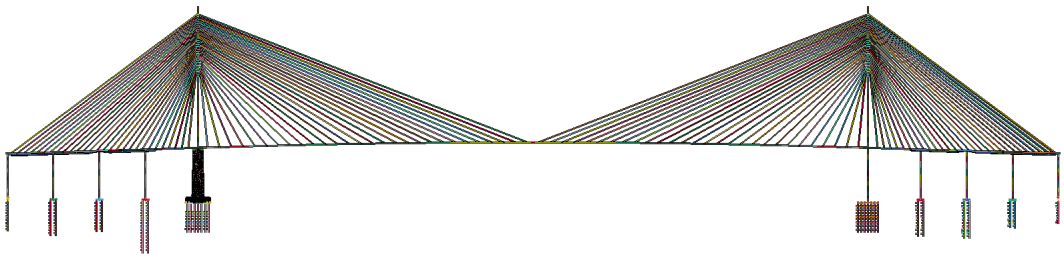

Fig. 5. FE model of the bridge.

The bridge's west tower is selected for ship impact. Plastic deformation and damage will occur on the tower legs and pile platform only. Therefore, the west tower leg and the pile platform connected with the tower leg are modelled in detail using fine meshes, as shown in Fig. 6 and Fig. 7. The entire bridge model contains 357,674 elements and 124,804 nodes. The present multi-scale modeling strategy can capture the detailed plastic deformation in the concerned regions and achieve high computational efficiency.

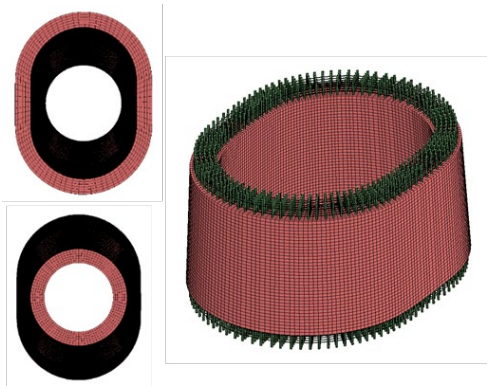

Fig. 6. Bridge tower model.

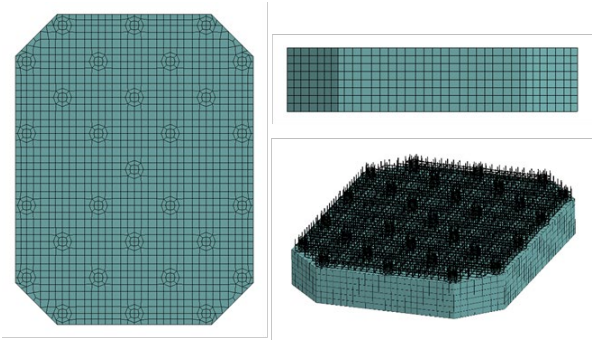

Fig. 7. Pile platform model.

Given the large scale of the bridge, the mesh size sensitivity analysis of the entire bridge is difficult. As the tower subjected to ship collision is the main target of the present study, the tower is modelled with three grid sizes of 1 m, 0.5 m and 0.25 m. The numerical results show that the collision force time history obtained by the 0.5 m grid and the 0.25 m grid are very close with the relative error within 2%, while the error of the 1 m grid is relatively large. The 0.5-m grid mesh is thus used in the present paper.

### *3.1.2. Material model*

The HJC[47], TCK[48], and K&C (Karagozian and Case) models[49] have been developed to model the concrete material under impact loading. Among these models, the K&C model is the most widely accepted[50]. The model introduces three strength surfaces, namely, the initial yield, ultimate strength, and residual failure surfaces, to determine the initial yield, ultimate, and residual strengths of concrete under load, respectively. From the beginning of loading to concrete failure, three main stages exist: 1) the elastic stage: the stress point does not reach the initial yield surface (YIELD); 2) the strengthening stage: the stress point exceeds the initial yield strength surface, but does not reach the ultimate strength surface (MAX); and 3) the softening stage: the stress point reaches the ultimate strength surface, but does not reach the residual failure surface (RESIDUAL). The initial yield, ultimate strength, and residual failure surfaces are determined by Equations (1), (2), and (3), respectively.

$$\Delta\sigma_y = a_{0y} + \frac{P}{a_{1y} + a_{2y}P} \tag{1}$$

$$\Delta\sigma_m = a_0 + \frac{P}{a_1 + a_2 P} \tag{2}$$

$$\Delta\sigma_r = \frac{P}{a_{1f} + a_{2f}P} \tag{3}$$

where $P = -(\sigma_1 + \sigma_2 + \sigma_3)/3$, and $a_0$, $a_1$, $a_2$, $a_{0y}$, $a_{1y}$, $a_{2y}$, $a_{1f}$, and $a_{2f}$ are

the material parameters.

In this study, two kinds of concrete with axial compressive strengths of 28.8 and 60.0 MPa are used. Their densities are assumed to be 2400 and 2500 kg/m$^3$, respectively. The strength parameters are shown in Table 3.

Table 3. Concrete strength parameters.

| $f_c$ (MPa) | $a_{0y}(MPa)$ | $a_{1y}$ | $a_{2y}(MPa^{-1})$ | $a_0(MPa)$ | $a_1$ | $a_2(MPa^{-1})$ | $a_{1f}$ | $a_{2f}(MPa^{-1})$ |
|---|---|---|---|---|---|---|---|---|
| 28.8 | 8.556 | 0.9658 | 0.003733 | 13.24 | 0.6046 | 0.001292 | 0.4417 | 0.005132 |
| 60.0 | 17.83 | 0.9658 | 0.001792 | 27.58 | 0.6046 | 0.000620 | 0.4417 | 0.002463 |

Considering the strain rate effect of the material and element failure, the elastoplastic dynamic model proposed by the Cooper–Symonds formula[33] is used to simulate steel and reinforcement. Two different steel types, i.e., Q235 and Q345, are used in the bridge. For both types, the density, Poisson's ratio and Young's modulus are 7700 kg/m$^3$, 0.2 and 200 GPa, respectively. Yield strength is 235 MPa for Q235 and 310 MPa for Q345.

### *3.1.3. Comparison of natural frequencies*

A modal analysis of the bridge is performed to verify the accuracy of the FE model. The first 20 natural frequencies calculated (with and without piles) are listed in Table 4 and compared with the measured counterparts. The calculated natural frequencies from the model without piles are consistent with those with piles. As expected, the former is slightly higher than the latter as the former has a higher stiffness than the latter. The first three natural frequencies measured are very near the calculation counterparts, verifying the accuracy of the FE model. The higher modes have some difference because the actual bridge contains complicated damping and boundary conditions that are difficult to model.

Table 4. Comparison of natural frequencies.

| Mode No. | Measurement (Hz) | LS-DYNA model (without piles) | LS-DYNA model (with piles) |
|---|---|---|---|
| 1 | 0.1606 | 0.157 | 0.1553 |
| 2 | 0.2117 | 0.2089 | 0.2084 |
| 3 | – | 0.2107 | 0.209 |
| 4 | – | 0.2219 | 0.2176 |
| 5 | 0.2500 | 0.2562 | 0.2553 |
| 6 | 0.2489 | 0.3298 | 0.2855 |
| 7 | 0.3233 | 0.3332 | 0.3321 |
| 8 | 0.4500 | 0.3781 | 0.3777 |
| 9 | 0.4028 | 0.3844 | 0.3787 |
| 10 | 0.3350 | 0.3966 | 0.3959 |
| 11 | 0.4617 | 0.463 | 0.4621 |
| 12 | 0.5033 | 0.517 | 0.491 |
| 13 | – | 0.5338 | 0.5158 |
| 14 | 0.4517 | 0.5841 | 0.5299 |
| 15 | 0.5967 | 0.6009 | 0.5328 |
| 16 | 0.6550 | 0.6114 | 0.5963 |
| 17 | 0.6583 | 0.6238 | 0.6155 |
| 18 | 0.7067 | 0.6606 | 0.6339 |
| 19 | 0.5517 | 0.6606 | 0.644 |
| 20 | 0.6767 | 0.6811 | 0.6772 |

### *3.2. Ship model*

Considering the real navigation situation around the cable-stayed bridge, ships of four different dead weight tonnages (DWT), namely, 2,700, 12,000, 30,000, and 75,000 DWT, are studied. The basic parameters of the four ships are listed in Table 5.

The bow shape and structure greatly affect the accuracy of calculation. To obtain a reliable collision force and the dynamic responses of the bridge, fine mesh sizes are adopted to model the bow structure, including the deck, the bulkhead, and the outer panel, as shown in Fig. 8. The elastoplastic dynamic hardening model is applied to the

material of the bow. Meanwhile, the middle and rear parts of the hull, which are far from the collision zone, are modeled using a coarse mesh to improve the calculation efficiency. The bow and the mid-rear hull are connected by node constraints.

In the ship-bridge collision problem, the influence of the water medium around the hull on the collision motion cannot be ignored. In order to improve the calculation efficiency, the additional water quality method can be used to deal with the influence of the water fluid, namely, the influence of the surrounding water medium is simplified into the form of the additional mass of the hull. In this paper, the attached water quality is taken as 0.05 times the ship's quality.

Table 5. Basic parameters of the ship.

| DWT (t) | 2,700 | 12,000 | 30,000 | 75,000 |
|---|---|---|---|---|
| Full load mass (t) | 3,350 | 18,930 | 44,687 | 115,000 |
| Additional mass (t) | 168 | 946 | 2,234 | 5,750 |
| Total length (m) | 106 | 141 | 241 | 300 |
| Width (m) | 17.6 | 22.6 | 32.3 | 40.9 |
| Depth (m) | 5.5 | 11.3 | 19 | 22.4 |
| Full load draught (m) | 3.5 | 8.3 | 11.5 | 13 |
| Bow form | V shape | Bulbous bow | Bulbous bow | Bulbous bow |
| Steel type | Q235 | Q235 | Q345 | Q345 |

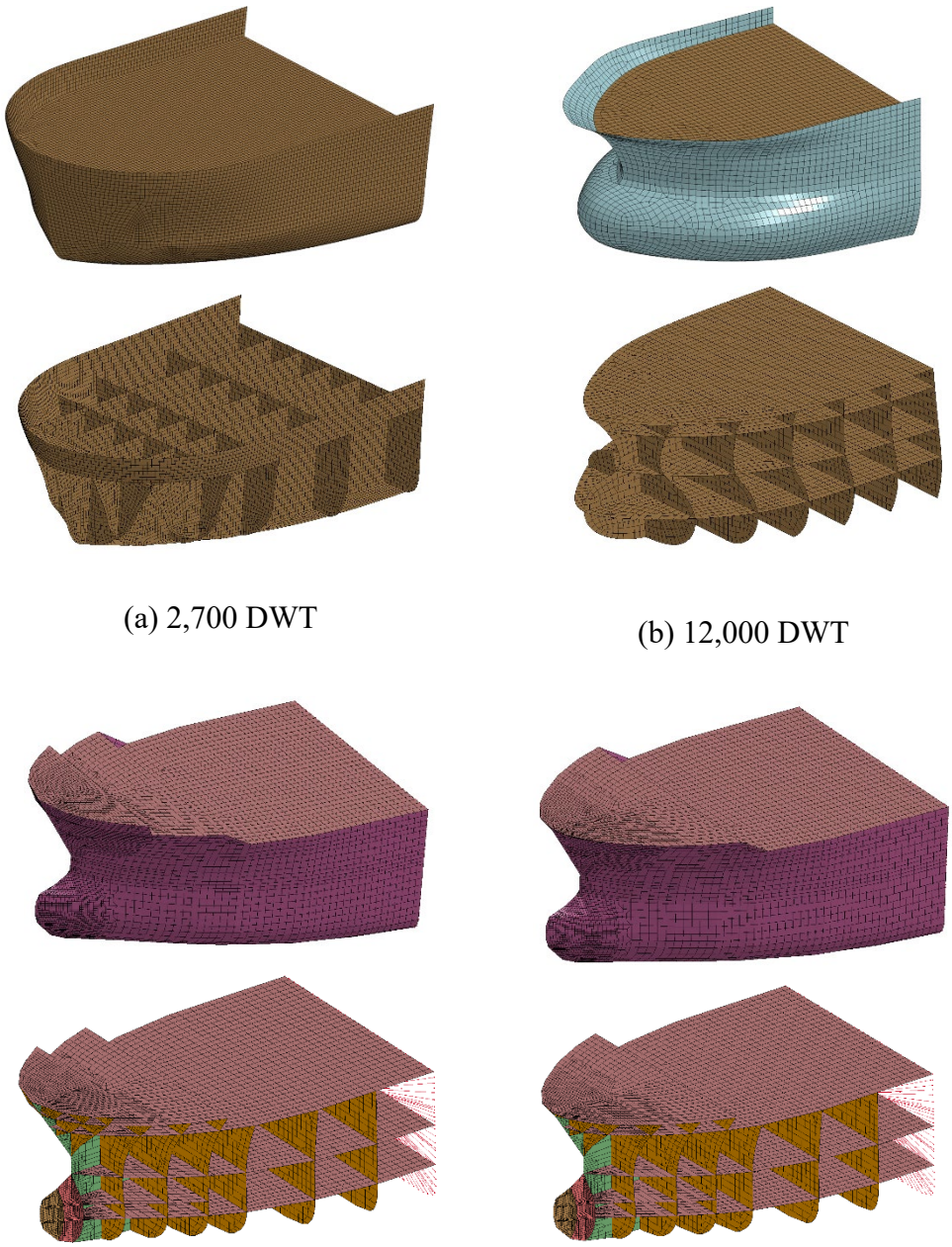

(a) 2,700 DWT (b) 12,000 DWT

(c) 30,000 DWT (d) 75,000 DWT

Fig. 8. FE models of the bow and inner structure of each ship type.

## 4. Ship–bridge collision simulation and collision force analysis

### *4.1. Impact velocity*

Existing empirical formulas of the collision force in ship–bridge collisions indicate that ship tonnage and the initial velocity of ship collision are the most basic parameters

affecting the collision force and the dynamic response of the bridge. Thus, for each of the four tonnages above, six impact velocities, namely, 1, 2, 3, 4, 5, and 6 m/s, are studied. The collision direction is assumed in the transverse bridge direction, which is perpendicular to the length of the bridge. The simulation process is divided into two stages: the first stage includes 0 s to 9 s within which gravity is applied through stress initialization, and the second stage simulates the ship–bridge collision process from 9 s. The stress time history of some typical gauge points in the first stage are shown in Fig. 9. It shows that the stress reaches a stable state at about 9 sec. Only the second stage of simulation is discussed in the present paper.

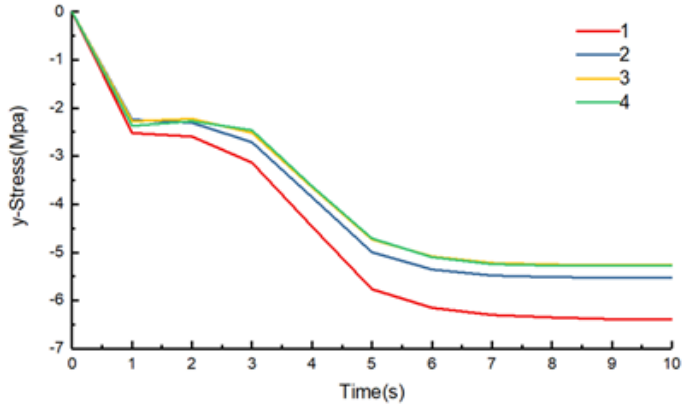


Fig. 9. Stress time history of some typical gauge points in the first stage.

### *4.2. Numerical collision force*

Using the FE models of the bridges and ship, the collision process of different DWTs, and the impact velocities, the ship–bridge collision process is simulated in LS-DYNA. The surface-to-surface contact is used in the present paper. Surface-to-surface contact is generally used for the interaction between structures or components, and the action area is large and the shape of the action area is uncertain. The program will check whether the slave surface node penetrates the main surface after each time step is solved. If no penetration occurs, the calculation continues. Otherwise, the program will apply a force in the direction along the normal line of the main surface to prevent further penetration of the nodes from the surface. The force applied is the contact force.

The time-history curves of the collision forces in different scenarios are shown in Fig. 10. The figure shows that the shape, the duration, and the maximum value of the collision force vary significantly under different ship tonnages and initial speeds. Furthermore, the collision force exhibits obvious nonlinear fluctuation characteristics because of the continuous yielding of the bow's steel plate during collision and the damage of the concrete part of the bridge tower. The fluctuation amplitude increases with the collision speed. During the collision process, the collision force increases to a peak value and then unloads to zero, indicating the end of collision.

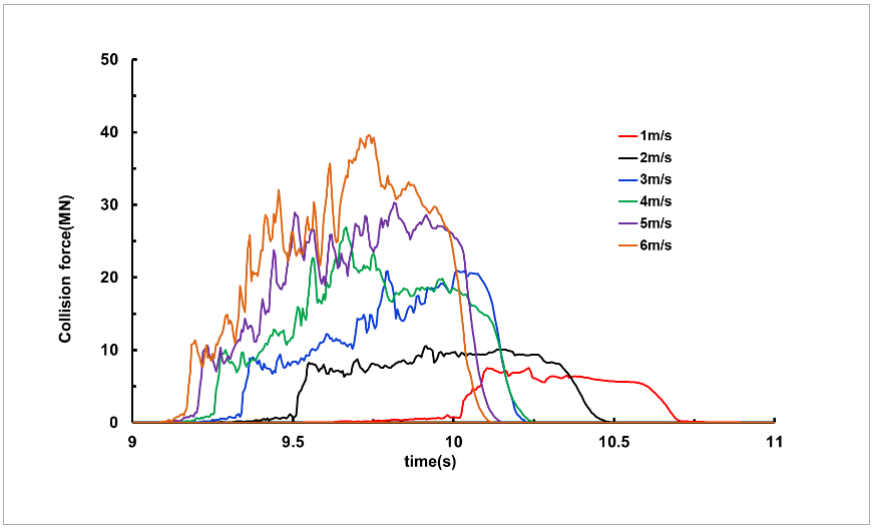


(a) 2,700 DWT

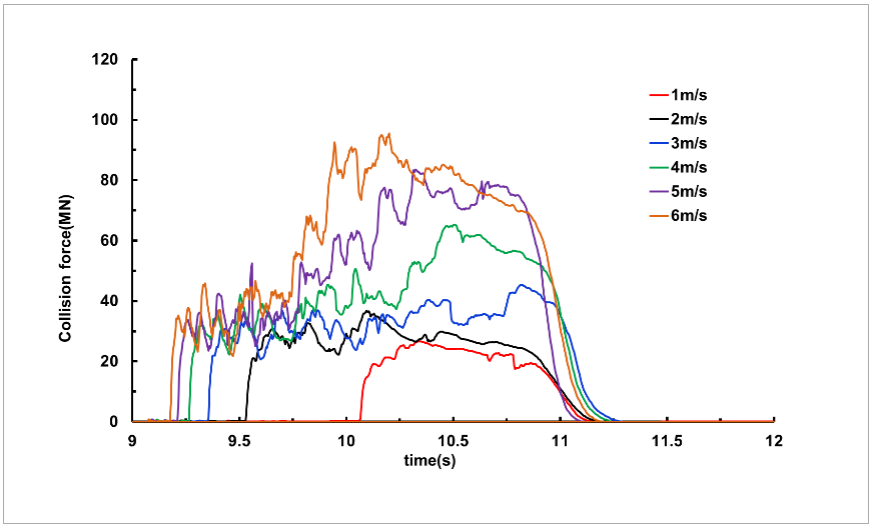


(b) 12,000 DWT

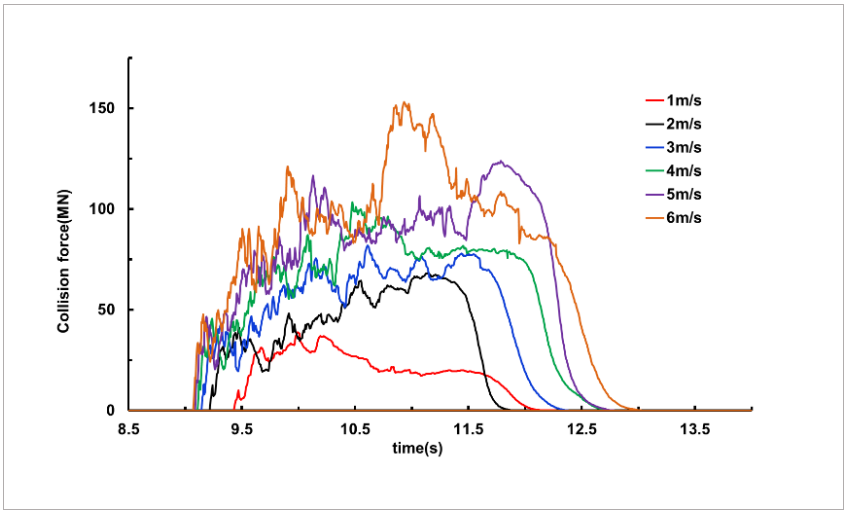


(c) 30,000 DWT

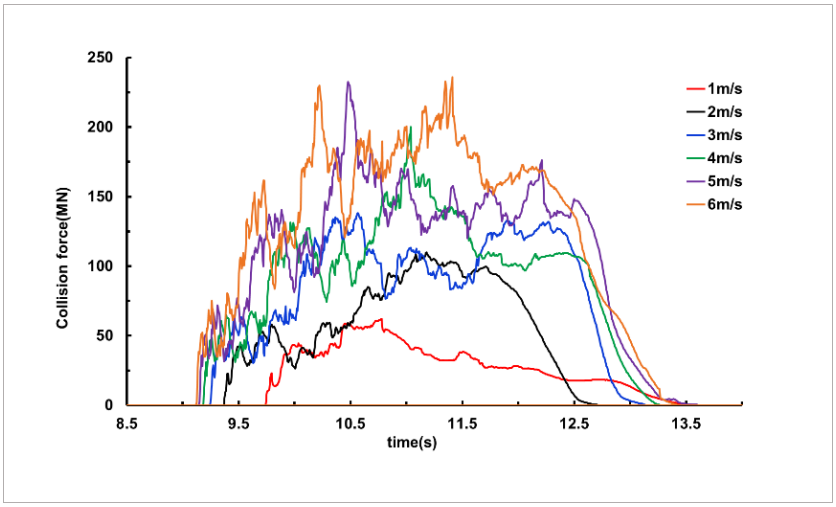


(d) 75,000 DWT

Fig. 10. Collision force time history in different cases.

### *4.3. Comparison of collision force between simulation and design codes*

According to Woisin et al.'s research work on the collision of a bow against a rigid wall, the AASHTO Standard[14] proposes a revised formula for calculating the collision force of forward bows against piers. The formula is applicable when bulk carrier, cargo ship, and tanker types of ship hit the pier in front. The equation is as follows:

$$P_t = 0.98\sqrt{DWT}\left(V/8\right), \tag{4}$$

where $P_t$ is the equivalent collision force (MN), and $V$ is the impact velocity (m/s).

Eurcode1 2.7[15] suggests the following collision force formula:

$$P = V\sqrt{KM}\ , \tag{5}$$

where $P$ is the equivalent collision force, $K$ is the equivalent stiffness of the impact ship (5 MN/m for inland ships and 15 MN/m for ocean ships), and $M$ is the mass of the ship in $10^6$ kg.

The China railway code[51] calculates the ship collision force as

$$F = \gamma v \sin\alpha \sqrt{\frac{W}{C_1 + C_2}}, \tag{6}$$

where $F$ is the equivalent collision force, $v$ is the impact velocity, $\gamma$ is a coefficient (oblique impact takes 0.2, normal impact takes 0.3), $\alpha$ is the collision angle, $W$ is the weight of the ship in MN, and $C_1$, and $C_2$ are coefficients and assumed to satisfy $C_1 + C_2 = 0.0005 m/kN$ in the absence of information.

For the present ship collision of different tonnages, the relationship between the calculated collision force and speed is shown in Fig. 11 and compared with different design codes. The comparison shows that in all tonnage cases, different codes provide quite different collision forces. The China railway code provides the smallest forces, while the European code (ocean ship) the largest. Furthermore, the European code (ocean ship) predicts the largest collision forces accurately in all cases, and the European code (inland ship) predicts the average collision forces with good accuracy.

The calculated forces using the AASHTO code are between the maximum and average collision forces. Considering that the specification calculates the average collision force of the ship hitting the bridge, the calculation results are overestimated because the formula is based on the impact test of ships over 40,000 tons and rigid walls. The collision force may be overestimated for small tonnage ships, such as the 2,700 DWT and 12,000 DWT ships in this study. In cases of large tonnage and high-speed ships, the

rigid wall tests ignore the damage to the collision object and material failure, leading to a large collision force. The results of the 30,000 DWT and 75,000 DWT ships provide evidence of this finding; the AASHTO code provides a similar force as the simulation as the ship at speed of 1 m/s and 2 m/s and higher results than the simulation ones when the speed exceeds 3 m/s.

The China railway code provides the smallest forces because the experimental data on the ship and pier's elastic deformation coefficients (C1 and C2 in Eq. (6)) are insufficient, and the code recommended values are adopted. The recommended coefficients are based on the research on a ship with a small rigidity, producing small collision force results.

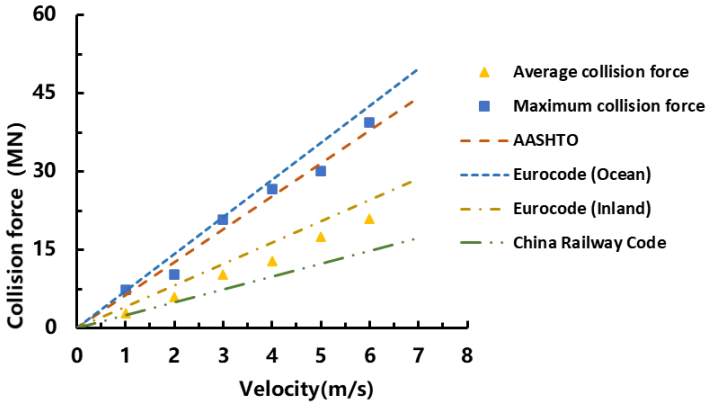


(a) 2,700 DWT

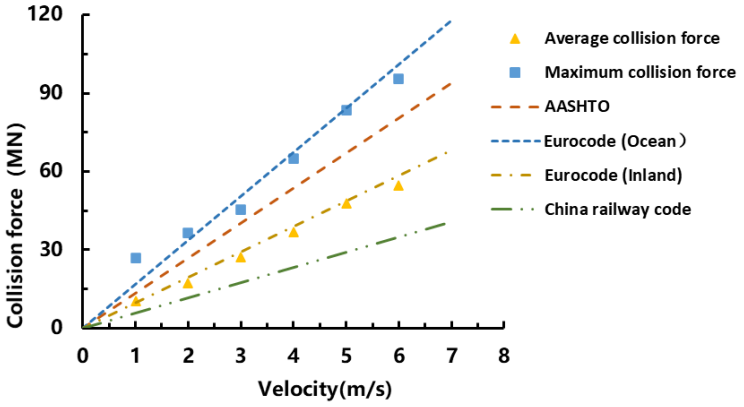


(b) 12,000 DWT

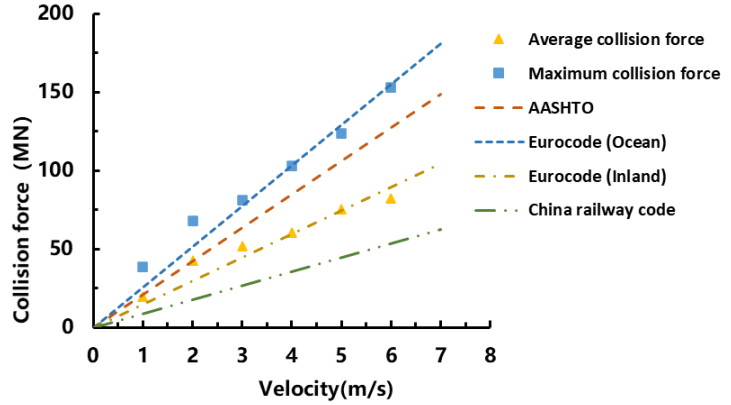


(c) 30,000 DWT

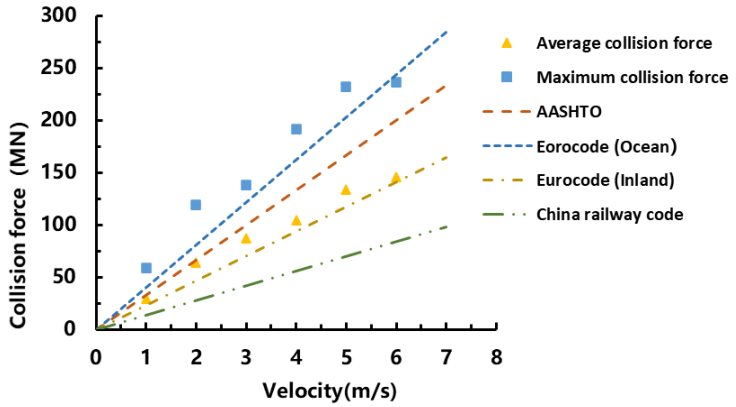


(d) 75,000 DWT

Fig. 11. Collision force time history in different cases.

### *4.4. Influence of concrete material model*

The pier may be regarded as a rigid body or an elastic body for simplification. For comparison, rigid body, elastic and K&C model are adopted to model the concrete material. Elastic modulus of elastic constitutive model is assumed to be $3.65\times10^4$ MPa. Collision force-time history of different material models at different impact velocities is compared in Fig. 12.

When the impact velocity is 2 m/s, the time-history curves obtained by the rigid body and linear elasticity assumptions are almost the same, with the peak collision force of 123.2 MN. The peak collision force using the K&C model is 119.3 MN, slightly smaller

than that of the other two models. In this case, the rigid body and elastic body assumptions can accurately estimate the peak collision force of the bridge. Because of the large stiffness of the bridge tower and the small collision speed of the ship, the concrete does not show serious damage and plastic deformation. Thus, the calculated peak collision force is not greatly affected by the material assumptions.

When the impact speed increases to 5 m/s, the collision force-time history of the bridge tower of three different materials is shown in Fig. 12(b). In the first second of the collision, the collision forces of the three models are almost the same. This is because at the beginning of the collision, the rigidity and strength of the concrete are relatively large, and the bridge structure does not have time to respond. Consequently, the difference in the material properties has little effect on the collision force. One second after the collision, the linear elastic model and the K&C model begin to undergo large deformation, while the K&C model quickly suffers severe plastic damage under the large impact force. Some concrete begin to withdraw from work. The effect of the material model difference on the collision force gradually appears. The three curves have two most obvious peaks. Regarding the material models of rigid body, elastic and K&C model, the first peak occurs at 10.45 s, 10.47 s and 10.48 s with the value of 227.93 MN, 219.7 MN and 232.0 MN, respectively. The second peak occurs at 11.89 s, 12.19 s and 12.21 s with the corresponding value of 248.5 MN, 244.9 MN and 176.3 MN, respectively. As the collision continues, the elastic deformation of the elastic pier continues to increase, the plastic deformation and destruction area of the bridge tower using the K&C model also further expands. The difference of the peak collision force increases, especially for the K&C model case.

When the impact velocity is 6 m/s, as shown in Fig. 12(c), the calculation results of the three models are more different. The maximum impact force obtained from the rigidity and elasticity assumptions are 26.5% and 23.3% higher than that of the K&C model, respectively. At this time, if one continues to use the rigid hypothesis or elastic hypothesis, the calculated collision force will be overestimated.

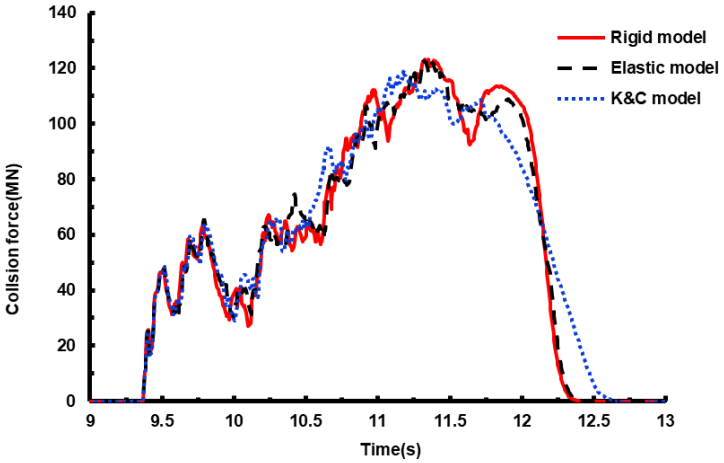
Rigid model
Elastic model
K&C model
Collsion force(MN)
Time(s)
0
20
40
60
80
100
120
140
9
9.5
10
10.5
11
11.5
12
12.5
13

(a) 2 m/s

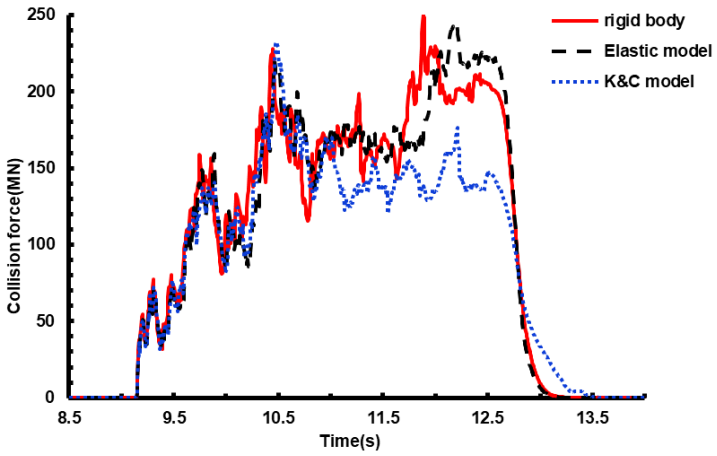
rigid body
Elastic model
K&C model
Collision force(MN)
Time(s)
0
50
100
150
200
250
8.5
9.5
10.5
11.5
12.5
13.5

(b) 5 m/s

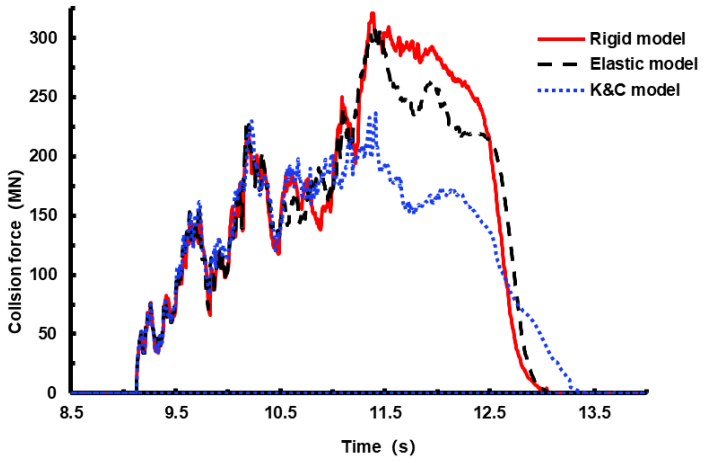


(c) 6 m/s

Fig. 12. Collision force-time history of different material models.

## 5. Bridge responses and local damage

### *5.1. Bridge responses*

As the west tower is directly subjected to ship collision, the position of tower top A, the connection point (B) between the bridge tower and the deck, and pile top C, as shown in Fig. 13, are chosen as the three critical points. Points D, E, and F in the east tower are also selected for comparison. The connection between the side span deck and the tower, point N, is also critical. In addition, points 1, 2, 3, 4, and 5 on the steel bridge deck of the main span are also chosen. Gauge point 3 is located in the middle of the span.

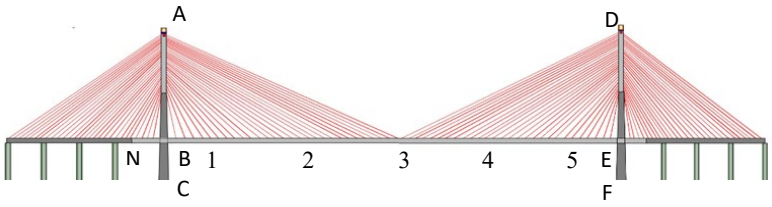


Fig. 13. Key points on the bridge.

The cable-stayed bridge mainly undergoes transverse displacement under ship collision. The maximum displacement of the tower occurs at the top of the struck bridge tower (point A). The maximum displacement of the main span bridge deck occurs at the mid-span position (point 3). The maximum transverse displacement of points A, N, and 3 for the cases of different ship DWTs and speeds are listed in Table 6. Under the same condition, the relationship between the maximum displacement of the three key points remains unchanged, namely, point A has the largest displacement and point N the smallest. As expected, the displacement increases with the ship mass and impact velocity. The displacements of point A versus the maximum and average collision forces are plotted in Fig. 14 and Fig. 15, respectively. The displacement is nearly linear with the collision force.

Table 6. Maximum transverse displacement of the bridge.

| DWT(t) | Velocity (m/s) | Maximum displacement (m) | | |
|---|---|---|---|---|
| | | A | N | 3 |
| 2700 | 1 | 0.0182 | 0.0033 | 0.0082 |
| 2700 | 2 | 0.0212 | 0.0043 | 0.0102 |
| 2700 | 3 | 0.0368 | 0.0075 | 0.0163 |
| 2700 | 4 | 0.0404 | 0.0092 | 0.0177 |
| 2700 | 5 | 0.0556 | 0.0112 | 0.0226 |
| 2700 | 6 | 0.0671 | 0.0146 | 0.0272 |
| 12000 | 1 | 0.0459 | 0.0112 | 0.0184 |
| 12000 | 2 | 0.0453 | 0.0128 | 0.0233 |
| 12000 | 3 | 0.0756 | 0.0156 | 0.0289 |
| 12000 | 4 | 0.1069 | 0.0202 | 0.0413 |
| 12000 | 5 | 0.1472 | 0.0306 | 0.0516 |
| 12000 | 6 | 0.1452 | 0.0390 | 0.0597 |
| 30000 | 1 | 0.0583 | 0.0143 | 0.0345 |
| 30000 | 2 | 0.1390 | 0.0254 | 0.0617 |
| 30000 | 3 | 0.1740 | 0.0324 | 0.0886 |
| 30000 | 4 | 0.1825 | 0.0361 | 0.0916 |
| 30000 | 5 | 0.2159 | 0.0533 | 0.1301 |
| 30000 | 6 | 0.2131 | 0.0518 | 0.1321 |
| 75000 | 1 | 0.0638 | 0.0243 | 0.0456 |
| 75000 | 2 | 0.1903 | 0.0434 | 0.0927 |
| 75000 | 3 | 0.2895 | 0.0654 | 0.1366 |
| 75000 | 4 | 0.2958 | 0.0686 | 0.1819 |
| 75000 | 5 | 0.3687 | 0.0833 | 0.2101 |
| 75000 | 6 | 0.3764 | 0.09832 | 0.2321 |

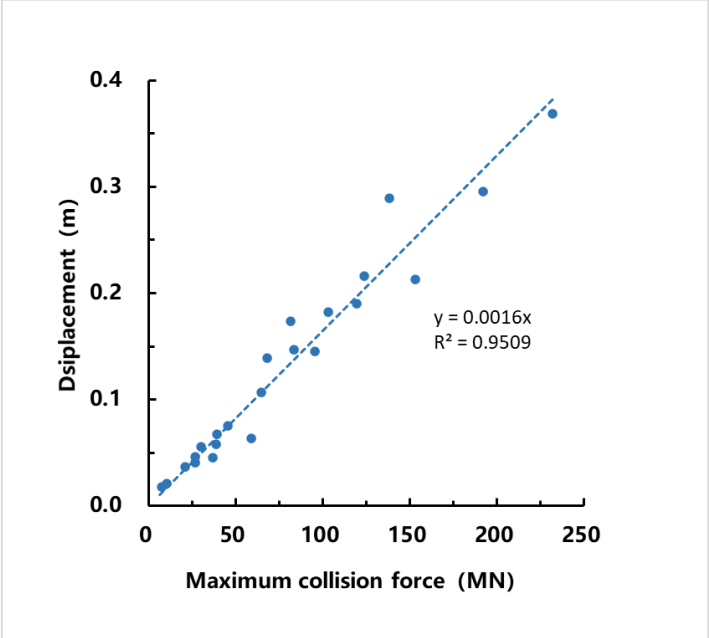


Fig. 14. Relationship between displacement and maximum collision force (Point A).

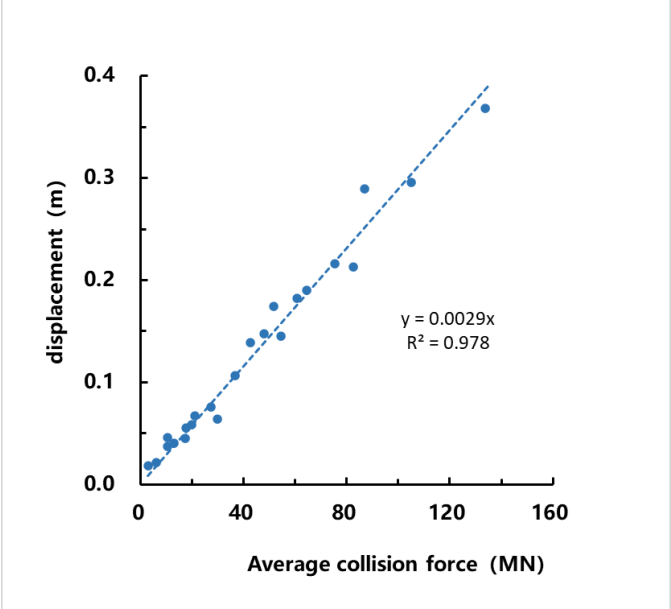


Fig. 15. Relationship between displacement and average collision force (Point A).

Taking the case of the 75,000 DWT ship at the speed of 5 m/s as an example, the displacement of each key point is analyzed. Fig. 16 shows the transverse displacement time history of the main tower. The displacement of the impacted west tower is significantly larger than that of the east tower. The tower top has a maximum

displacement, while the bottom of the platform has the smallest displacement. Fig. 17 shows the transverse displacements at points 1–5 (shown in Fig. 13) of the main span of the bridge deck. The mid-span experiences maximum displacement.

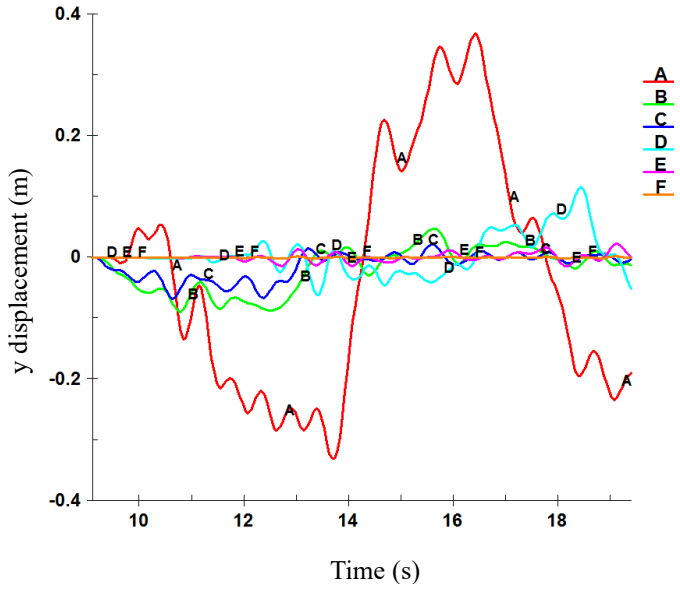


Fig. 16. Transverse displacement of the main tower.

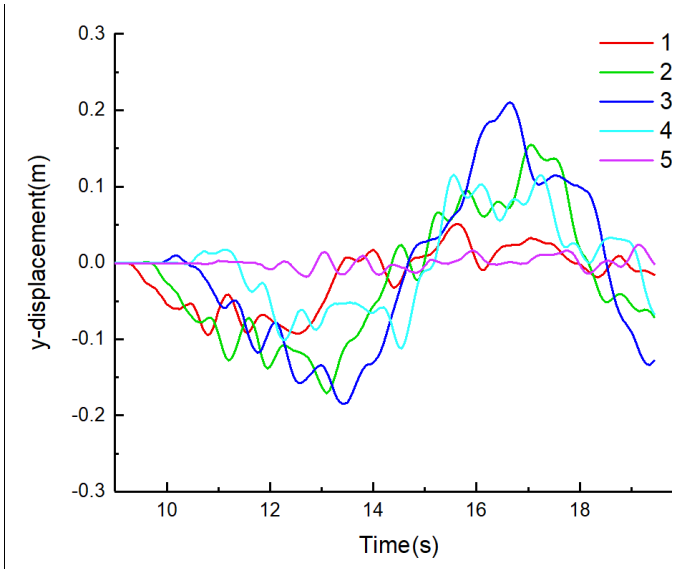


Fig. 17. Transverse displacement of the bridge deck.

### *5.2. Local damage of the bridge tower*

Taking the case of the 75,000-DWT ship hitting the bridge tower at a speed of 5 m/s as an example, the development of the local damage of the bridge tower is studied. Figs, 18, 19, and 20 are the respective screenshots of the ship–bridge collision process, the bridge tower damage, and the equivalent plastic strain of the bow at some critical moments during the collision.

At 9.1 s, the bulbous bow of the ship begins to touch the bridge tower. Currently, only a small part of the concrete in the contact area begins to enter the hardening stage, which does not cause damage to other parts and an obvious overall response. As the ship continues to move forward, the upper part of the bow also contacts the bridge tower, and the collision force reaches the maximum value at 10.5 s. At this time, two areas on the surface of the bridge tower in contact with the bow have severe damage. The concrete on the side and bottom of the bridge tower also show slight damage, and the overall response of the bridge is significant. The collision force reaches the maximum value at 10.5 s, but this is not the moment of the worst concrete damage. As the collision continues, the contact area between the bow and the bridge tower further increases, the damage range of the concrete continues to expand, and the second peak value of maximum collision force occurs at 12.2 s. At this instant, many concrete units on the surface of the bridge tower are fully damaged, vertical cracks appear on both sides of the bridge tower, and serious damages appear on the bottom of the bearing platform. After reaching the second main peak, the collision force enters the rapid unloading stage. Currently, the damage of the concrete continues to develop, and the vertical cracks on the two sides extend upward and downward. A vertical crack also appears in the middle of the front of the bridge tower. Until 13.4 s, the ship completely separates from the bridge tower, indicating the end of the collision, and the damage of the bridge tower stops developing.

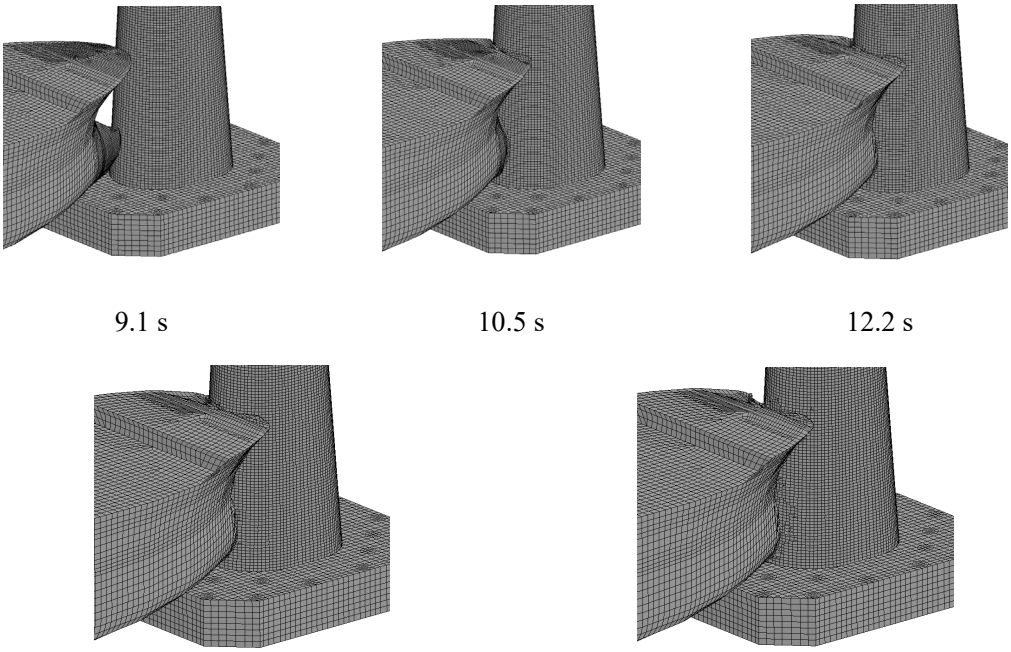


Fig. 18. Ship–bridge collision process.

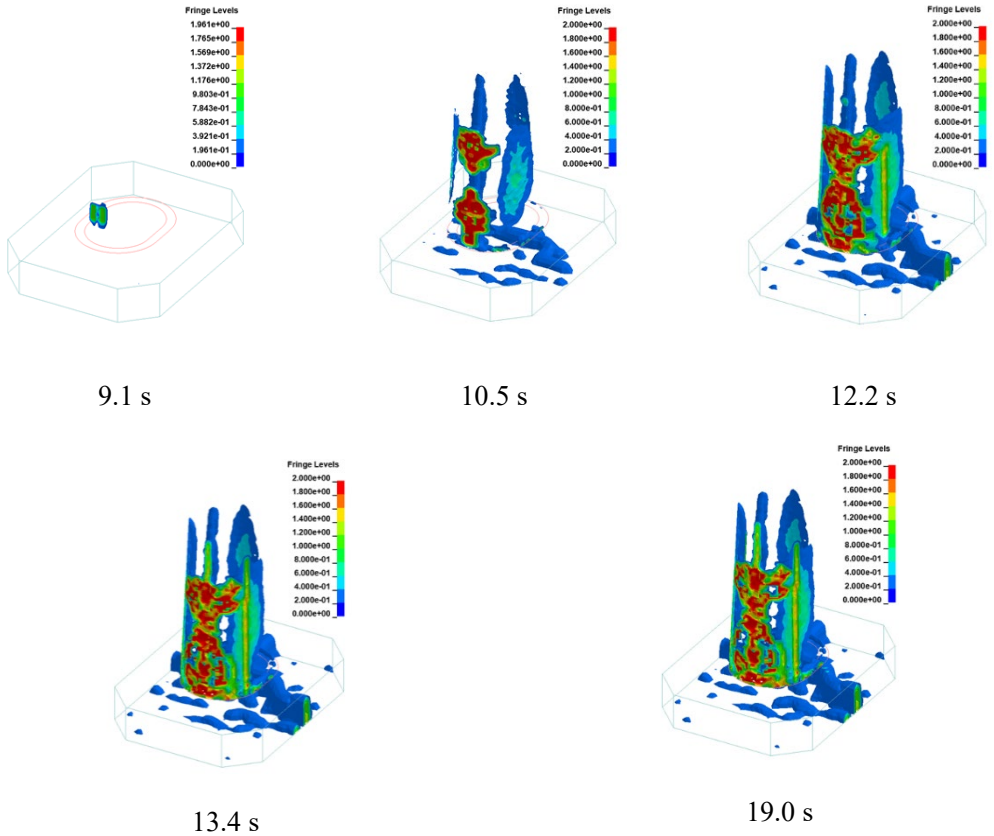


Fig. 19. Dynamic damage process of the bridge tower.
(75,000-DWT ship at a speed of 5 m/s)

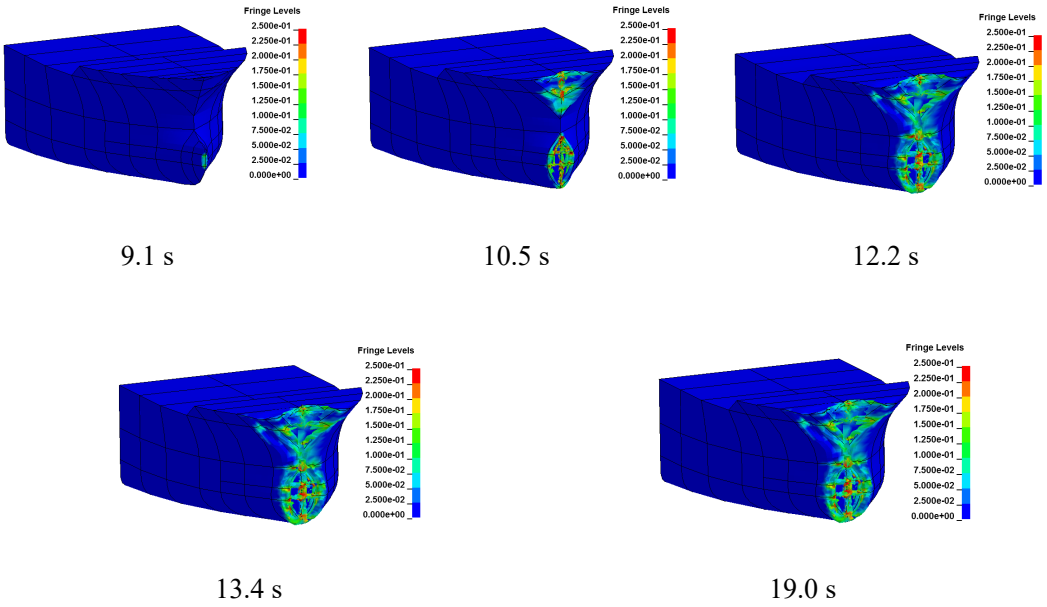


Fig. 20. Equivalent plastic strain of the ship bow.

## 6. Conclusions

The FE simulation is adopted to comprehensively study the mechanical properties of a long-span cable-stayed bridge under various ship collision scenarios. The simulation provides a reasonable collision force prediction to facilitate the design and evaluation of bridges. Following conclusions can be drawn from the numerical simulation:

1. The calculated collision force (both maximum and average collision forces) is mainly affected by the impact velocity and the mass of the ship. Collision force has a linear relationship with impact velocity. The calculated collision forces are compared with different design codes, which show a significant difference. Among the design codes, Eurocode provides reasonable collision force predictions.
2. Different material models are adopted in the simulation. When the initial kinetic energy of the ship is small, the rigid body or elastic material can be used to replace the concrete material of the bridge tower for the ship collision analysis, and the accurate collision force time history can be obtained. However, when the initial

kinetic energy of the ship is large, the rigid body or elastic assumption may overestimate the collision force.

3. The cable-stayed bridge mainly undergoes transverse displacement under the ship–bridge collision. The maximum horizontal displacement of the bridge tower occurs at the top of the impacted bridge tower, and the maximum displacement of the main span deck occurs at the mid-span. The maximum displacement at these locations has a linear relationship with the average collision force.

**Acknowledgment**

This work was supported by the National Natural Science Foundation of China (Project No. 51678364).

## References


1 Y. Yang, Y. Ge, R. Zhou, S. Chen and L. Zhang, Aerodynamic Countermeasure Schemes of Super Long-Span Suspension Bridges with Various Aspect Ratios, *Int. J. Struct. Stab. Dyn.* **20**(05) (2020) 2050061.

2 X. Chen, R. Hu, H. Tang, Y. Li, E. Yu and L. Wang, Flutter Stability of a Long-Span Suspension Bridge During Erection in Mountainous Areas, *Int. J. Struct. Stab. Dyn.* **20**(09) (2020) 2050102.

3 S. Huang, Q. Li, M. Liu, F. Chen and S. Liu, Numerical Simulation of Wind-Driven Rain on a Long-Span Bridge, *Int. J. Struct. Stab. Dyn.* **19**(12) (2020) 1950149.

4 Q. Pu, J. Liu, H. Gou, Y. Bao and H. Xie, Finite element analysis of long-span rail-cum-road cable-stayed bridge subjected to ship collision, *Adv. Struct. Eng.* **22**(11) (2019) 2530-2542.

5 K. Wardhana and F.C. Hadipriono, Analysis of recent bridge failures in the United States, *J. Perform. Constr. Facil.* **17**(3) (2003) 144-150.

6 I. E. Harik, A. M. Shaaban, H. Gesund, G. Y. S. Valli and S. T. Wang, United States bridge failure 1951–1988, *J. Perform. Constr. Facil.* **4**(4) (1990) 272–277.

7 L. P. Perera and C. G. Soares, Collision risk detection and quantification in ship navigation with integrated bridge systems, *Ocean Eng.* **109**(15) (2015) 344–354.

8 M. W. Whitney, I. E. Harik, J. J. Griffin, D. L. Allen, Barge collision design of highway bridges, *J. Bridge Eng.* **1**(2) (1996) 47–58.

9 SCMP, *https://www.scmp.com/news/hong-kong/economy/article/1871482/ hong-kong-traffic-chaos-tsing-ma-bridge-closes-leaving*, (2015).

10 V. U. Minorsky, An Analysis of Ship Collisions with Reference to Protection of Nuclear Power Plants, *J. Ship Res.* **3** (1959) 1-4.

11 G. Woisin, The collision tests of the GKSS, *Jahrbuch der Schiffbautechnischen Gesellschaft*, **70** (1976) 465–487.

12 O. D. Larsen, Ship Collision with Bridges: The Interaction between Vessel Traffic and Bridge Structures, *IABSE Structural Engineering Document 4*, IABSE-AIPC-IVBH, Zürich, Switzerland. (1993).

13 M. Knott and Z. Pruca, Vessel collision design of bridges, *Bridge Engineering Handbook*, W.-F. Chen and L. Duan (eds.), CRC Press, Boca Raton, Chapter 60, (2000).

14 AASHTO, *Guide Specification and Commentary for Vessel Collision Design of Highway Bridges*, American Association of State Highway and Transportation Officials, Washington, D.C. (1991).

15 European Committee for Standardization, EN 1991-1-7:2006, *Actions on structures Part 1.7: General actions, Accidental actions,* Brussels, (2006).

16 Norwegian Public Roads Administration. L*oad Regulations for Bridges and Ferry Ramps in the Public Road System,* Preliminary Edition, Olso, (1986).

17 Nordic Road Engineering Federation. *Load Regulations for Bridge.* NVF, Report No.4, (1980).

18 K. E. Meir-Dornberg,. Ship collisions, safety zones, and loading assumptions for structures in inland waterways. *VDI-Berichte*, **496**(1) (1983) 1–9.

19 A. W. Vredeveldt and L.J. Wevers, Full-scale ship collision tests, *Proceedings of First Conference on Marine Safety and Environment Ship production*, Netherland. 1-5 June (1992) 743–769.
20 G. R. Consolazio, R.A. Cook and G. B. Lehr, *Barge Impact Testing of the St. George Island Causeway Bridge*, University of Florida Report, (2002).
21 P. Yuan and I. E. Harik, One-dimensional model for multi-barge flotillas impacting bridge piers, *Comput.-Aided Civil Infrastruct. Eng.* **23**(6) (2008) 437–447.
22 P. Yuan and I. E. Harik, Equivalent barge and flotilla impact forces on bridge piers, *J. Bridge Eng.* **15** (2009) 523–32.
23 Y. Sha and H. Hao, Nonlinear finite element analysis of barge collision with a single bridge pier, *Eng. Struct.* **41**(2012) 63–76.
24 Y. Sha and H. Hao, Laboratory tests and numerical simulations of barge impact on circular reinforced concrete piers, *Eng. Struct.* **46**(2013) 593-605.
25 Y. Sha and H. Hao, A simplified approach for predicting bridge pier responses subjected to barge impact loading, *Adv. Struct. Eng.* **17**(1) (2014) 11–23.
26 Y. Sha, J. Amdahl and C. Dørum, Dynamic responses of a floating bridge subjected to ship collision load on bridge girders, *Procedia Engineering* **199**(2017) 2506–2513.
27 Y. Sha, J. Amdahl and K. Liu, Design of steel bridge girders against ship forecastle collisions, *Eng. Struct.* **196**(2019) 109277.
28 J. Zhang, X. Chen, D. Liu, and X. Li, Analysis of bridge response to barge collision: refined impact force models and some new insights, *Adv. Struct. Eng.* **19**(8) (2016) 1224–1244.
29 B. Liu and C. G. Soares, Assessment of the strength of double-hull tanker side structures in minor ship collisions, *Eng. Struct.* **120**(2016):1–12.
30 D. Servis, M. Samuelides, T. Louka and G. Voudouris, Implementation of finite-element codes for the simulation of ship-ship collisions. *J. Ship Res.* **46**(2002) 239–247.
31 P. Hogström and J. W. Ringsberg, Assessment of the crashworthiness of a selection of innovative ship structures. *Ocean Eng.* **59**(2013) 58–72.
32 G. R. Consolazio and D. R. Cowan, Nonlinear analysis of barge crush behavior and its relationship to impact resistant bridge design, *Comput. Struct.* **81**(8–11) (2003) 547-557.
33 LSTC, *LS-DYNA Theory Manual.* Livermore, CA: Livermore Software Technology Corporation, (2006).
34 LSTC, *LS-DYNA Keyword User's Manual,* Livermore, CA: Livermore Software Technology Corporation, (2007).
35 X. Guo, C. Zhang, and Z. Chen, Dynamic performance and damage evaluation of a scoured double-pylon cable-stayed bridge under ship impact. *Eng. Struct.* **216** (2020) 110772.
36 G. Gholipour, C. Zhang, and A. A. Mousavi, Effects of axial load on nonlinear response of RC columns subjected to lateral impact load: Ship-pier collision. *Eng. Fail. Anal.* **91** (2018) 397-418.
37 G. Gholipour, C. Zhang, and A. A. Mousavi, Analysis of girder bridge pier

subjected to barge collision considering the superstructure interactions: the case study of a multiple-pier bridge system. *Struct. Infrastruct. Eng.* **15** (3) (2019) 392-412.

38 G. Gholipour, C. Zhang, W. H. Kang, and A. A. Mousavi, Reliability analysis of girder bridge piers subjected to barge collisions. *Struct. Infrastruct. Eng.* **15**(9) (2019) 1200-1220.

39 G. Gholipour, C. Zhang, and A. A. Mousavi, Nonlinear numerical analysis and progressive damage assessment of a cable-stayed bridge pier subjected to ship collision. *Mar Struct*. **69** (2020) 102662.

40 C. Zhang, G. Gholipour, and A. A. Mousavi, State-of-the-Art Review on Responses of RC Structures Subjected to Lateral Impact Loads. *Arch. Comput. Method Eng.* (2020). 1- 31.

41 W. Fan, Y. Sun, C.C. Yang, W.B. Sun, and Y. He, Assessing the response and fragility of concrete bridges under multi-hazard effect of vessel impact and corrosion", *Eng. Struct.* **225** (2020) 111279

42 K. Oppong, D. Saini, and B. Shafei, Vulnerability Assessment of Bridge Piers Damaged in Barge Collision to Subsequent Hurricane Events. *J. Bridge Eng.* **25**(8) (2020) 04020051.

43 W. Fan, W. Guo, Y. Sun, B.S. Chen and X. D. Shao, Experimental and numerical investigations of a novel steel-UHPFRC composite fender for bridge protection in vessel collisions, *Ocean Eng.* **165** (2018) 1-21.

44 W. Fan, D. J. Shen, X. Huang, and Y. Sun, Reinforced concrete bridge structures under barge impacts: FE modeling, dynamic behaviors, and UHPFRC-based strengthening, *Ocean Eng.* **216** (2020) 108116.

45 H. Hao and E. K. C. Tang, Numerical simulation of a cable-stayed bridge response to blast loads, Part II: Damage prediction and FRP strengthening, *Eng. Struct.* **32** (10) (2010) 3193-3205.

46 E. K. C. Tang and H. Hao, Numerical simulation of a cable-stayed bridge response to blast loads, Part I: Model development and response calculations, *Eng. Struct.* **32** (10) (2010) 3180-3192.

47 T. J. Holmquist, G. R. Johnson and W. H. Cook, A computational constitutive model for concrete subjected to large strains, high strain rates and high pressures, *Proceeding of 14th International Symposium on Ballistics*, Qubec, Canada: 1591-1995. (1993).

48 L. M. Taylor, E. P. Chen and J. S. Kuszmaul, Micro-crack induced damage accumulation in brittle rock under dynamic loading, *Comput Methods Appl Mech Eng.*, 55(3)(1986) 301-320.

49 L. J. Malvar, J. E. Crawford, J. W. Wesevich and J. W. Wesevich, A Plasticity Concrete Material Model for DYNA 3D, *J Impact Eng.*, **19**(9-10)(1997) 847-873.

50 T. V. Do, T. M. Pham and H. Hao, Impact force profile and failure classification of reinforced concrete bridge columns against vehicle impact, *Eng. Struct.* **183**(2019) 443-458.

51 The Third Survey and Design Institute of the Ministry of Railways, *Basic Specifications for the Design of Railway Bridges and Culverts*, China Railway

Publishing House, (2000). (in Chinese)